Optik - International Journal for Light and Electron Optics 290 (2023) 171128

Contents lists available at ScienceDirect

Optik

journal homepage: www.elsevier.com/locate/ijleo

Original research article

Design of tilted and decentered anamorphic optical system based on nodal aberration control

Xu Zhang [a,b], Liping Wang [a,c,d], Jie Yu [a,c,d], Chunshui Jin [a,c,d,*]

[a] Changchun Institute of Optics, Fine Mechanics and Physics, Chinese Academy of Sciences, Changchun, Jilin 130033, China
[b] University of Chinese Academy of Sciences, Beijing 100039, China
[c] State Key Laboratory of Applied Optics, Changchun, Jilin 130033, China
[d] Key Laboratory of Optical System Advanced Manufacturing Technology, Chinese Academy of Sciences, Changchun, Jilin 130033, China

ARTICLE INFO

Keywords:
Optical design
Anamorphic system
Tilted and decentered system

ABSTRACT

This paper proposes a design method for tilted and decentered anamorphic projection optics. In this method, the structure is designed in groups according to the magnification requirements; the anamorphic system section's primary aberration is analyzed based on vector aberration theory, the tilted and decentered system section's node behavior is analyzed based on node aberration theory, and spatial ray tracing is used to control the anamorphic optical system's pupil to be elliptical to realize pupil matching between groups. A mathematical aberration balance and constraint control model is established. The node position is used as an evaluation function such that the node is close to or within the full field, thus controlling the primary aberration for the initial system over the full field. The initial system is constructed with increased optimization potential to satisfy the aberration and structural constraints. The initial structure for the tilted and decentered anamorphic projection optics ($\beta_x = 1/4, \beta_y = 1/8$) is constructed with the coma and astigmatism nodes close to or within the full field. The structure is then optimized to achieve a wavefront root-mean-square error for the EUV tilted and decentered anamorphic objective with NA= 0.55 of better than 0.025λ ($\lambda = 13.5$ nm).

1. Introduction

The tilted and decentered system is widely used in off-axis optical systems. In the EUV field, tilted and decentered elements provide systems greater freedom to achieve very small aberrations. With lithography technology gaining traction for operation at the 5–3 nm node, the extreme ultraviolet (EUV) lithography projection optics, which form the core element of the exposure system, are being developed with higher numerical apertures [1–3]. To balance the impact of these high numerical apertures on shadowing effects and on the system's productivity, anamorphic objective systems with demagnifications of 4 × in the orthogonal scanning direction (*x*-direction) and 8 × in the scanning direction (*y*-direction), will have to be applied in high-numerical-aperture (high-NA) EUV lithography optical systems. EUV lithography projection optics have very high imaging requirements and are required to achieve resolutions beyond the diffraction limit [1]. Different types of aberrations in the projection optics affect different lithography performance indicators, and an appropriate initial structure for aberration balance can help to optimize the control of each aberration in

* Corresponding author at: Changchun Institute of Optics, Fine Mechanics and Physics, Chinese Academy of Sciences, Changchun, Jilin 130033, China.
E-mail address: jincs@sklao.ac.cn (C. Jin).

https://doi.org/10.1016/j.ijleo.2023.171128
Received 7 March 2023; Received in revised form 16 May 2023; Accepted 29 June 2023
Available online 4 July 2023
0030-4026/© 2023 Published by Elsevier GmbH.

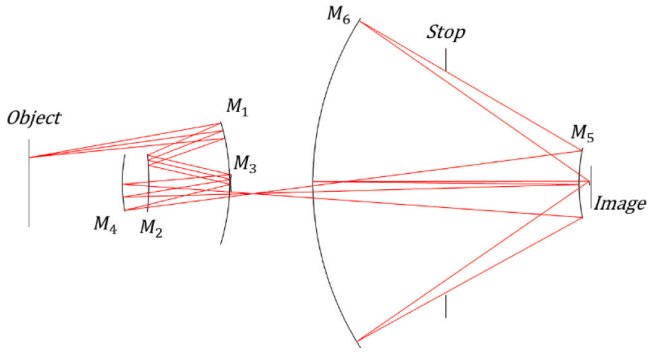

Fig. 1. Schematic diagram of the tilted and decentered anamorphic optical system.

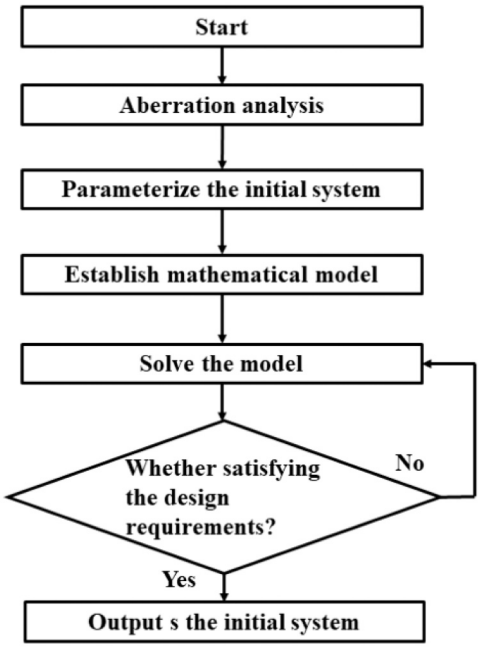

Fig. 2. Flow chart for the initial system design.

the optical system.

To design high-NA projection optics with different magnifications in the *X* and *Y* directions, Mann used the grouping design method described in their patent. The groupings were based on the aperture group and the field group, with the aperture group being selected as the non-anamorphic surface and the field group being selected as the anamorphic surface according to their design requirements, to ensure that the magnification requirements in the *X* and *Y* directions were met [4]. Li's team proposed a combined magnification method for design of the initial structure for high-NA (NA=0.5) projection optics that provided a solution for construction of the initial structure of the high-NA projection optics from the first-order structure direction, but it did not consider the primary aberration [5]. Jin's team used vector aberration theory when designing the initial structure of high-NA (NA=0.55) projection optics, and derived and calculated the third-order aberration coefficients of the co-axial anamorphic optical system elements to achieve aberration balance and multi-constraint control within the initial system [6].

The tilted and decentered elements provide greater freedom for the anamorphic optical system design to achieve high-NA EUV lithography projection optics with very small aberrations. All the design methods described above use optics with co-axial elements as their initial structure and add the tilted and decentered variables during the optimization process. These methods do not consider the effects of tilted and decentered elements on the aberrations in the initial optical system. This causes a large perturbation in the optimization process; the system deviates too widely from the initial system, the constraint is difficult to control, and the system can easily fall into a local minimal value. To ensure balance between the aberrations and the multi-constraint control of the initial system for tilted and decentered anamorphic optical systems, this paper proposes an initial system design method for these optical systems. First, the method groups the systems according to their magnification requirements, and it then controls the aberration values of the

anamorphic system components based on vector aberration theory to prevent the initial system from having excessively large primary aberration values. Using nodal aberration theory, the nodal behavior of the tilted and decentered system aberrations, which include spherical aberrations, coma aberrations, and astigmatism, is analyzed to ensure that the nodes remain within the required field as far as possible to reduce the system's aberrations. Spatial ray tracing is used to control the pupil shape of the anamorphic optical system and realize pupil matching between the groups. Second, the optical system's structural constraints and aberrations are parameterized, and a mathematical model of the tilted and decentered anamorphic optical system is then established to solve for the initial system, with the aberration node position acting as the evaluation function. Finally, an initial system design with optimization potential is provided for the tilted and decentered anamorphic optical system. In this paper, an initial tilted and decentered anamorphic projection optics system is constructed via this method. The nodes are either close to or within the full field, as shown by the field map of the coma aberrations and astigmatism. The initial system has a small full-field aberration value and is optimized to achieve a wavefront root-mean-square (RMS) error for the EUV tilted and decentered anamorphic objective with NA= 0.55 of better than 0.025λ (where the wavelength $\lambda = 13.5$ nm).

2. Initial system design

In this paper, the tilted and decentered anamorphic optical system shown in Fig. 1 is divided into three groups for the initial system design. The design flow is as shown in Fig. 2. To satisfy the magnification requirements of the optical system in both the X and Y directions, the first group, M_1, M_2, and M_3, are coaxial elements with anamorphic conic surfaces, and the expression for Z is:

$$Z = \frac{c_x x^2 + c_y y^2}{1 + \sqrt{1 - \left(1 + k_x\right) c_x^2 x^2 - \left(1 + k_y\right) c_y^2 y^2}} \tag{1}$$

where c_x and c_y represent the curvatures of the XZ plane and the YZ plane, respectively, and k_x and k_y represent the cones of the XZ and YZ planes, respectively. To provide better connections to the subsequent elements, M_3 acts as the stop for G1. G1 is analyzed using the theory described in Section 2.1 part A. To increase the number of degrees of freedom of the optical system, the second group components M_4 and M_5 are tilted and decentered elements with conic surfaces, and the expression for Z in this case is:

$$Z = \frac{c\mathrm{r}^2}{1 + \sqrt{1 - (1 + k) c^2 \mathrm{r}^2}} \tag{2}$$

where c represents the surface curvature, r represents the polar diameter of the surface polar coordinates, respectively, and k represents the surface cones. G2 is then analyzed using the nodal aberration theory described in Section 2.1 part B. The third group is the stop and M_6, where M_6 is a coaxial element with a conic surface. The stop for the latter group is set between M_5 and M_6 to ensure the telecentricity of the system during the subsequent optimization. To calculate the co-axial aberration and the aberration nodes, the structure of each group will be parameterized according to paraxial theory. A mathematical model containing multiple constraints will then be established. The model will then be solved to obtain an initial system that meets the design requirements, as shown in Section 2.2.

2.1. Previous theory

A. Vector aberration theory for co-axial optical system with anamorphic conic surfaces.
Based on vector wave aberration theory [7–10]:

$$W = \sum_{j} \sum_{p}^{\infty} \sum_{n}^{\infty} \sum_{m}^{\infty} (W_{klm})_j \left(\vec{H} \cdot \vec{H}\right)^p (\vec{\rho} \cdot \vec{\rho})^n \left(\vec{H} \cdot \vec{\rho}\right)^m \tag{3}$$

The aberration of an anamorphic optical system is dependent on the field coordinates (H_x,H_y) and the pupil coordinates (ρ_x,ρ_y). The vector aberration of the anamorphic optical system can be obtained by substituting $\vec{H} = \vec{H}_x + \vec{H}_y$ and $\vec{\rho} = \vec{\rho}_x + \vec{\rho}_y$into Eq. (3) to give:

$$\begin{aligned} W_{klm} &= \sum_{j} \sum_{p} \sum_{n} \sum_{m} (W_{klm})_j \left(\vec{H} \cdot \vec{H}\right)^p (\vec{\rho} \cdot \vec{\rho})^n \left(\vec{H} \cdot \vec{\rho}\right)^m \\ &= \sum_{j} \sum_{p} \sum_{n} \sum_{m} (W_{klm})_j \left[\left(\vec{H}_x + \vec{H}_y\right) \cdot \left(\vec{H}_x + \vec{H}_y\right)\right]^p \left[(\vec{\rho}_x + \vec{\rho}_y) \cdot (\vec{\rho}_x + \vec{\rho}_y)\right]^n \left[\left(\vec{H}_x + \vec{H}_y\right) \cdot (\vec{\rho}_x + \vec{\rho}_y)\right]^m \\ &= \sum_{j} \sum_{p} \sum_{n} \sum_{m} (W_{klm})_j \left(H_x^2 + H_y^2\right)^p \left(\rho_x^2 + \rho_y^2\right)^n \left(H_x \cdot \rho_x + H_y \cdot \rho_y\right)^m \end{aligned} \tag{4}$$

where $k = 2p+m$ and $l= 2\,n + m$. When $k + l= 4$, Eq. (4) then represents the third-order aberration vector form. This form consists of six parameters: H_x^2,H_y^2,ρ_x^2,ρ_y^2,$H_x\rho_x$,$H_y\rho_y$. There are 21 terms for the third-order aberration of the anamorphic optical system, three of which are piston terms and two of which appear twice, which means that there are actually 16 terms in total for the third-order

aberration of the anamorphic optical system, as given in Eq. (5):

$$\begin{aligned} W(H_x,H_y;\rho_x,\rho_y) &= \left\{D_1\rho_x^4 + D_2\rho_y^4 + D_3\rho_x^2\rho_y^2\right\} \\ &+\left\{D_4H_x\rho_x^3 + D_5H_y\rho_x^2\rho_y + D_6H_x\rho_x\rho_y^2 + D_7H_y\rho_y^3\right\} \\ &+\left\{D_8H_x^2\rho_x^2 + D_9H_y^2\rho_y^2 + D_{10}H_y^2\rho_x^2 + D_{11}H_x^2\rho_y^2 + D_{12}H_xH_y\rho_x\rho_y\right\} \\ &+\left\{D_{13}H_x^3\rho_x + D_{14}H_y^3\rho_y + D_{15}H_xH_y^2\rho_x + D_{16}H_x^2H_y\rho_y\right\} \end{aligned} \tag{5}$$

Each third-order aberration coefficient for the anamorphic optical system is shown below in Eq. (6).

$$\begin{cases} D_1 = -\frac{1}{8}\sum_{j=1}^{k}\left\{\left[A_{x,j}\left(h_{x,j}\Delta u_{x,j}^2 + c_{x,j}h_{x,j}^2\Delta u_{x,j}\right)\right] + \left(c_{x,j}^3 - c_{3,j}^3\right)h_{x,j}^4\Delta n_j\right\} \\ D_2 = -\frac{1}{8}\sum_{j=1}^{k}\left\{\left[A_{y,j}\left(h_{y,j}\Delta u_{y,j}^2 + c_{y,j}h_{y,j}^2\Delta u_{y,j}\right)\right] + \left(c_{y,j}^3 - c_{5,j}^3\right)h_{y,j}^4\Delta n_j\right\} \\ D_3 = -\frac{1}{4}\sum_{j=1}^{k}\left\{\left[A_{x,j}\left(h_{x,j}\Delta u_{y,j}^2 + c_{y,j}h_{y,j}^2\Delta u_{x,j}\right)\right] + \left(c_{x,j}^2c_{y,j} - c_{4,j}^3\right)h_{x,j}^2h_{y,j}^2\Delta n_j\right\} \\ D_4 = -\frac{1}{6}\sum_{j=1}^{k}\left\{\left[A_{x,j}\left(\bar{h}_{x,j}\Delta u_{\mathrm{x},j}^2 + c_{x,j}h_{x,j}^2\Delta\bar{u}_{x,j} + 2h_{x,j}\Delta u_{x,j}\bar{u}_{x,j} + 2c_{x,j}h_{x,j}\bar{h}_{x,j}\Delta u_{x,j}\right) - \psi_x\Delta u_{\mathrm{x},j}^2 + 3\left(c_{x,j}^3 - c_{3,j}^3\right)h_{x,j}^3\bar{h}_{x,j}\Delta n_j\right]\right\} \\ D_5 = -\frac{1}{2}\sum_{j=1}^{k}\left\{\left[A_{x,j}\left(h_{x,j}\Delta u_{y,j}\bar{u}_{y,j} + c_{y,j}h_{y,j}\bar{h}_{y,j}\Delta u_{x,j}\right) + \left(c_{x,j}^2c_{y,j} - c_{4,j}^3\right)h_{x,j}^2h_{y,j}\bar{h}_{y,j}\Delta n_j\right]\right\} \\ D_6 = -\frac{1}{2}\sum_{j=1}^{k}\left\{\left[A_{x,j}\left(\bar{h}_{x,j}\Delta u_{y,j}^2 + c_{y,j}h_{y,j}^2\Delta\bar{u}_{x,j}\right) - \psi_x\Delta u_{\mathrm{y},j}^2 + \left(c_{x,j}^2c_{y,j} - c_{4,j}^3\right)h_{x,j}\bar{h}_{x,j}h_{y,j}^2\Delta n_j\right]\right\} \\ D_7 = -\frac{1}{6}\sum_{j=1}^{k}\left\{\left[A_{y,j}\left(\bar{h}_{y,j}\Delta u_{y,j}^2 + c_{y,j}h_{y,j}^2\Delta\bar{u}_{y,j} + 2h_{y,j}\Delta u_{y,j}\bar{u}_{y,j} + 2c_{y,j}h_{y,j}\bar{h}_{y,j}\Delta u_{y,j}\right) - \psi_y\Delta u_{\mathrm{y},j}^2 + 3\left(c_{y,j}^3 - c_{5,j}^3\right)h_{y,j}^3\bar{h}_{y,j}\Delta n_j\right]\right\} \\ D_8 = -\frac{1}{4}\sum_{j=1}^{k}\left\{\left[A_{x,j}\left(h_{x,j}\Delta\bar{u}_{\mathrm{x},j}^2 + c_{x,j}\bar{h}_{x,j}^2\Delta u_{x,j} + 2\bar{h}_{x,j}\Delta u_{x,j}\bar{u}_{x,j} + 2c_{x,j}h_{x,j}\bar{h}_{x,j}\Delta\bar{u}_{x,j}\right) - 2\psi_x\Delta u_{x,j}\bar{u}_{x,j} + 3\left(c_{x,j}^3 - c_{3,j}^3\right)h_{x,j}^2\bar{h}_{x,j}^2\Delta n_j\right]\right\} \\ D_9 = -\frac{1}{4}\sum_{j=1}^{k}\left\{\left[A_{y,j}\left(h_{y,j}\Delta\bar{u}_{\mathrm{y},j}^2 + c_{y,j}\bar{h}_{y,j}^2\Delta u_{y,j} + 2\bar{h}_{y,j}\Delta u_{y,j}\bar{u}_{y,j} + 2c_{y,j}h_{y,j}\bar{h}_{y,j}\Delta\bar{u}_{y,j}\right) - 2\psi_y\Delta u_{y,j}\bar{u}_{y,j} + 3\left(c_{x,j}^3 - c_{3,j}^3\right)h_{x,j}^2\bar{h}_{x,j}^2\Delta n_j\right]\right\} \\ D_{10} = -\frac{1}{4}\sum_{j=1}^{k}\left\{\left[A_{x,j}\left(h_{x,j}\Delta\bar{u}_{y,j}^2 + c_{y,j}\bar{h}_{y,j}^2\Delta u_{x,j}\right)\right] + \left(c_{x,j}^2c_{y,j} - c_{4,j}^3\right)h_{x,j}^2\bar{h}_{y,j}^2\Delta n_j\right\} \\ D_{11} = -\frac{1}{4}\sum_{j=1}^{k}\left\{\left[A_{y,j}\left(h_{y,j}\Delta u_{x,j}^2 + c_{x,j}h_{x,j}^2\Delta u_{y,j}\right)\right] + \left(c_{x,j}c_{y,j}^2 - c_{4,j}^3\right)\bar{h}_{x,j}^2h_{y,j}^2\Delta n_j\right\} \\ D_{12} = -\sum_{j=1}^{k}\left\{\left[A_{x,j}\left(\bar{h}_{x,j}\Delta u_{y,j}\bar{u}_{y,j} + c_{y,j}h_{y,j}\bar{h}_{y,j}\Delta\bar{u}_{x,j}\right) - \psi_x\Delta u_{y,j}\bar{u}_{y,j} + \left(c_{x,j}^2c_{y,j} - c_{4,j}^3\right)h_{x,j}\bar{h}_{x,j}h_{y,j}\bar{h}_{y,j}\Delta n_j\right]\right\} \\ D_{13} = -\frac{1}{2}\sum_{j=1}^{k}\left\{\left[A_{x,j}\left(\bar{h}_{x,j}\Delta\bar{u}_{x,j}^2 + c_{x,j}\bar{h}_{x,j}^2\Delta\bar{u}_{x,j}\right) - \psi_x\Delta\bar{u}_{x,j}^2 + \left(c_{x,j}^3 - c_{3,j}^3\right)h_{x,j}\bar{h}_{x,j}^3\Delta n_j\right]\right\} \\ D_{14} = -\frac{1}{2}\sum_{j=1}^{k}\left\{\left[A_{y,j}\left(\bar{h}_{y,j}\Delta\bar{u}_{y,j}^2 + c_{y,j}\bar{h}_{y,j}^2\Delta\bar{u}_{y,j}\right) - \psi_y\Delta\bar{u}_{y,j}^2 + \left(c_{y,j}^3 - c_{5,j}^3\right)h_{y,j}\bar{h}_{y,j}^3\Delta n_j\right]\right\} \\ D_{15} = -\frac{1}{2}\sum_{j=1}^{k}\left\{\left[A_{x,j}\left(\bar{h}_{x,j}\Delta\bar{u}_{y,j}^2 + c_{y,j}\bar{h}_{y,j}^2\Delta\bar{u}_{x,j}\right) - \psi_x\Delta\bar{u}_{y,j}^2 + \left(c_{x,j}^2c_{y,j} - c_{4,j}^3\right)h_{x,j}\bar{h}_{x,j}\bar{h}_{y,j}^2\Delta n_j\right]\right\} \\ D_{16} = -\frac{1}{2}\sum_{j=1}^{k}\left\{\left[A_{y,j}\left(\bar{h}_{y,j}\Delta\bar{u}_{x,j}^2 + c_{x,j}\bar{h}_{x,j}^2\Delta\bar{u}_{y,j}\right) - \psi_y\Delta\bar{u}_{x,j}^2 + \left(c_{x,j}^2c_{y,j} - c_{4,j}^3\right)\bar{h}_{x,j}^2h_{y,j}\bar{h}_{y,j}\Delta n_j\right]\right\} \end{cases} \tag{6}$$

where the parameter relationships are given by:

$$\begin{cases} A_{x,j} = n_j u_{x,j} + n_j h_{x,j} c_{x,j} \\ \overline{A}_{x,j} = n_j \overline{u}_{x,j} + n_j \overline{h}_{x,j} c_{x,j} \\ A_{y,j} = n_j u_{y,j} + n_j h_{y,j} c_{y,j} \\ \overline{A}_{y,j} = n_j \overline{u}_{y,j} + n_j \overline{h}_{y,j} c_{y,j} \end{cases} \begin{cases} c_{3,j} = \sqrt[3]{\left(1 + k_{x,j}\right) c_{x,j}^3} \\ c_{4,j} = \sqrt[3]{\frac{1}{2}\left[\left(1 + k_{x,j}\right) c_{x,j}^2 c_{y,j} + \left(1 + k_{y,j}\right) c_{x,j} c_{y,j}^2\right]} \\ c_{5,j} = \sqrt[3]{\left(1 + k_{y,j}\right) c_{x,j}^3} \end{cases} \begin{cases} \psi_x = n_j\left(\overline{h}_{x,j} u_{x,j} - h_{x,j} \overline{u}_{x,j}\right) \\ \psi_y = n_j\left(\overline{h}_{y,j} u_{y,j} - h_{y,j} \overline{u}_{y,j}\right) \end{cases} \tag{7}$$

where $(h_{x,j}, u_{x,j})$ and $(\overline{h}_{x,j}, \overline{u}_{x,j})$ denote the height and angle parameters for the paraxial marginal ray and the chief ray, respectively, in the x-direction on the j_{th} surface; $(h_{y,j}, u_{y,j})$ and $(\overline{h}_{y,j}, \overline{u}_{y,j})$ denote the height and angle parameters for the paraxial marginal ray and the chief ray, respectively, in the y-direction on the j_{th} surface; $c_{x,j}$ and $c_{y,j}$ represent the curvatures of surface j on the XZ and YZ planes, respectively; and $k_{x,j}$ and $k_{y,j}$ represent the cones of surface j on the XZ and YZ planes, respectively.

Because the terms in the Zernike polynomial correspond to the third-order aberration, it follows that when the Zernike polynomial is used to represent astigmatism that [11]:

$$W = \left(W_{2,2}^{2,0} H_x^2 + W_{2,2}^{0,2} H_y^2\right) Z_2^2\left(\rho_x, \rho_y\right) + \left(W_{-2,2}^{1,1} H_x H_y\right) Z_2^{-2}\left(\rho_x, \rho_y\right) \tag{8}$$

If one direction in the system is corrected for astigmatism or if the curve is of degree two, it means that there is only one type of astigmatism, which is represented by either Z_2^2 or Z_2^{-2}. When the term $W_{-2,2}^{1,1} H_x H_y$ is zero, the field map of the astigmatism then describes either two crossing lines oriented parallel to the coordinate axes or a hyperbola with principal axes parallel to the coordinate axes. When the term $W_{2,2}^{2,0} H_x^2 + W_{2,2}^{0,2} H_y^2$ is zero, the field map of the astigmatism describes a hyperbola and its principal axes are not parallel to the coordinate axes.

B. Nadal aberration theory for a tilted and decentered optical system with conic surfaces.

According to the Nadal aberration theory introduced by Thompson [12], the wave aberrations for nonrotationally symmetrical systems are built on a vectorial formulation. The decentered field's contribution to each surface should be described by introducing a displacement vector $\overrightarrow{\sigma}_j$. The displacement vector $\overrightarrow{\sigma}_j$ can be divided into the vector $\overrightarrow{\sigma}_{spherej}$ for the spherical surface contribution and the vector $\overrightarrow{\sigma}_{asphere j}$ for the aspheric surface contribution, as follows:

$$\overrightarrow{\sigma}_{spherej} = -\frac{\left[\overrightarrow{N}_j \times \left(\overrightarrow{R}_j \times \overrightarrow{S}_j\right)\right]}{\overline{u}_j + \overline{h}_j c_j} \tag{9}$$

$$\overrightarrow{\sigma}_{asphere j} = \frac{\delta v_j^*}{\overline{h}_j} \tag{10}$$

where $\overrightarrow{N}_j$ is the surface normal vector of the local object; $\overrightarrow{R}_j$ is the direction of the optical axis ray (OAR) that is incident on the surface; $\overrightarrow{S}_j$ is the surface normal vector at the OAR intersection point; $\overrightarrow{u}_j$ is the chief ray angle at a surface j; $\overrightarrow{h}_j$ is the chief ray height at surface j; c_j is the curvature of surface j; and δv_j^* is the distance between the height of the aberration field symmetry axis and the heights of each of the optical axis rays on the aspheric surface relative to the reference axis after decentering and tilting.

The wave aberration expansion is represented by vectors as follows [13]:

$$W = \sum_j \sum_p^{\infty} \sum_n^{\infty} \sum_m^{\infty} (W_{klm})_j \left(\left(\overrightarrow{H} - \overrightarrow{\sigma}_j\right) \cdot \left(\overrightarrow{H} - \overrightarrow{\sigma}_j\right)\right)^p (\overrightarrow{\rho} \cdot \overrightarrow{\rho})^n \left(\left(\overrightarrow{H} - \overrightarrow{\sigma}_j\right) \cdot \overrightarrow{\rho}\right)^m \tag{11}$$

Then, after expanding the equation above, we obtain the third-order form:

$$\begin{aligned} W = {} & \Delta W_{20}\left(\overrightarrow{\rho} \cdot \overrightarrow{\rho}\right) + \Delta W_{11}\left(\overrightarrow{H} \cdot \overrightarrow{\rho}\right) + \sum_j W_{040j} (\overrightarrow{\rho} \cdot \overrightarrow{\rho})^2 \\ & + \sum_j W_{131j}\left[\left(\overrightarrow{H} - \overrightarrow{\sigma}_j\right) \cdot \overrightarrow{\rho}\right]\left(\overrightarrow{\rho} \cdot \overrightarrow{\rho}\right) + \sum_j W_{222j}\left[\left(\overrightarrow{H} - \overrightarrow{\sigma}_j\right) \cdot \overrightarrow{\rho}\right)\right]^2 \\ & + \sum_j W_{220j}\left[\left(\overrightarrow{H} - \overrightarrow{\sigma}_j\right) \cdot \left(\overrightarrow{H} - \overrightarrow{\sigma}_j\right)\right]\left(\overrightarrow{\rho} \cdot \overrightarrow{\rho}\right) \\ & + \sum_j W_{311j}\left[\left(\overrightarrow{H} - \overrightarrow{\sigma}_j\right) \cdot \left(\overrightarrow{H} - \overrightarrow{\sigma}_j\right)\right]\left[\left(\overrightarrow{H} - \overrightarrow{\sigma}_j\right) \cdot \overrightarrow{\rho}\right] \end{aligned} \tag{12}$$

where ΔW_{20} is the coefficient for focusing, ΔW_{11} is the coefficient for tilting, W_{040j} is the coefficient for the third-order spherical aberration, W_{131j} is the coefficient for a third-order coma, $W_{222j}$is the coefficient for a third-order astigmatism, $W_{220j}$is a coefficient related to the third-order component of the field curvature, and W_{311j} is the third-order distortion. , .

For a tilted and decentered optical system with conic surfaces, the nodal behavior of four third-order aberrations, comprising a

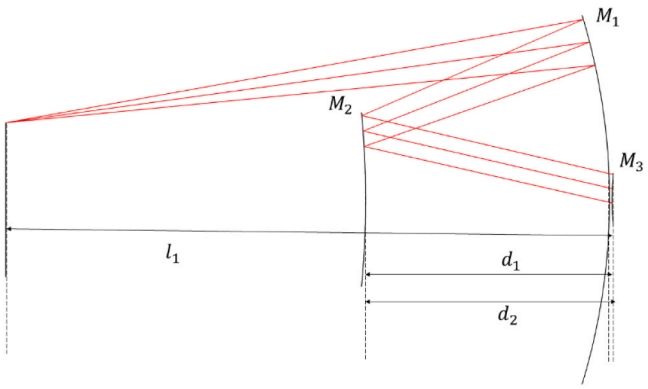

Fig. 3. Schematic diagram of Group 1.

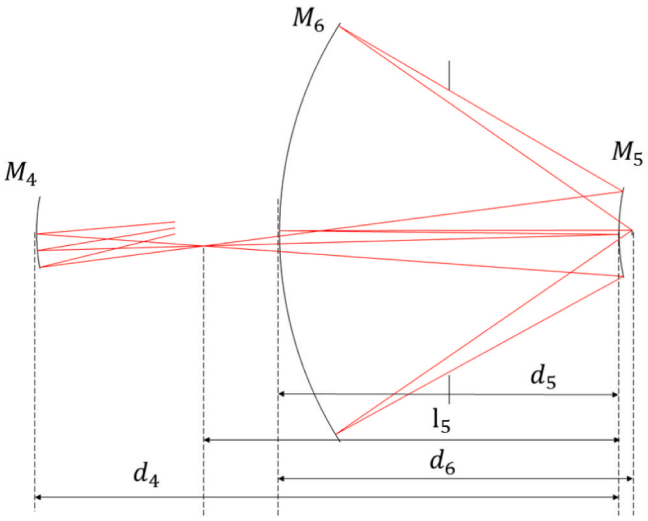

Fig. 4. Schematic diagram of Group 2 and Group 3.

spherical aberration, a coma, an astigmatism, and field curvature, is analyzed. The third-order spherical aberration is independent of the field vector $\vec{H}$ and is therefore unaffected by the only substitution required to invoke nonrotational symmetry. The third-order coma has a point in the field at which there is no coma and the field is determined using the vector $\vec{a}_{131}$. The normalized vector $\vec{a}_{131}$ is given as:

$$\vec{a}_{131} \equiv \left(\sum_j W_{131j}\vec{\sigma}_j\right) \Big/ W_{131} \tag{13}$$

If the third-order coma is corrected in a system, then this third-order coma will be constant in both magnitude and direction over the entire field of view. The third-order astigmatism has two points in the field at which there is no astigmatism. The normalized vector is then given as:

$$\vec{H}_{ast} \equiv \left(\sum_j W_{222j}\vec{\sigma}_j\right) \Big/ W_{222} \pm \left(- \left(\sum_j W_{222j}\vec{\sigma}_j^2\right) \Big/ W_{222} + \left(\left(\sum_j W_{222j}\vec{\sigma}_j\right) \Big/ W_{222} \right)^2 \right)^{1/2} \tag{14}$$

The characteristic field behavior for field curvature in an optical system without symmetry is for the vertex of the curvature to be decentered to a point located using the vector $\vec{a}_{220M}$ and to be defocused by an amount proportional to b_{220M}. The normalized vector is given by:

$$\vec{a}_{220M} \equiv \left(\sum_j W_{220Mj}\vec{\sigma}_j\right) \Big/ W_{220M}$$

$$b_{220M} \equiv \left(\sum_j W_{220Mj}\left(\vec{\sigma}_j \cdot \vec{\sigma}_j\right)\right) \Big/ W_{220M} - \vec{a}_{220M} \cdot \vec{a}_{220M} \tag{15}$$

$$W_{220M} = W_{220} + \frac{1}{2}W_{222}$$

The size of the focal shift is given by:

$$\delta z_{220M} = -8(f\#)^2 W_{220M} b_{220M} \tag{16}$$

where $f\#$ is the f-number of the optical system.

2.2. Grouping design

A. Group 1.

The quantities for Group 1 are defined as follows: l_1, d_1, d_2, and d_3 represent the lens thicknesses from object to M_1, M_1 to M_2, M_2 to M_3, and M_3 to M_4, respectively; $h_{x,1}$, $h_{x,2}$, and $h_{x,3}$, and $h_{y,1}$, $h_{y,2}$, and $h_{y,3}$ represent the paraxial marginal ray heights of the XZ and YZ planes at M_1, M_2, and M_3, respectively; and h_4 represents the paraxial marginal ray height at M_4. In addition, $r_{x,1}$, $r_{x,2}$, and $r_{x,3}$, and $r_{y,1}$, $r_{y,2}$, and $r_{y,3}$ represent the radii of curvature of the XZ and YZ planes at M_1, M_2, and M_3, respectively; and $k_{x,1}$, $k_{x,2}$, and $k_{x,3}$, and $k_{y,1}$, $k_{y,2}$, and $k_{y,3}$ represent the cones of the XZ and YZ planes at M_1, M_2, and M_3, respectively. Furthermore, $l_{x,1}$, $l_{x,2}$, and $l_{x,3}$, and $l_{y,1}$, $l_{y,2}$, and $l_{y,3}$ represent the object distances to the XZ and YZ planes at M_1, M_2, and M_3, respectively; l_4 represents the object distance at M_4; and $l'_{x,1}$, $l'_{x,2}$, and $l'_{x,3}$, and $l'_{y,1}$, $l'_{y,2}$, and $l'_{y,3}$ represent the image distances to the XZ and YZ planes at M_1, M_2, and M_3, respectively.

Based on the paraxial approximation, we now introduce the following parameters:

$$\begin{cases} \alpha_{x1} = \dfrac{l_{x2}}{l_{x1}'} \approx \dfrac{h_{x2}}{h_{x1}} \\ \alpha_{x2} = \dfrac{l_{x3}}{l_{x2}'} \approx \dfrac{h_{x3}}{h_{x2}} \\ \alpha_{x3} = \dfrac{l_4}{l_{x3}'} \approx \dfrac{h_4}{h_{x3}} \end{cases} \begin{cases} \alpha_{y1} = \dfrac{l_{y2}}{l_{y1}'} \approx \dfrac{h_{y2}}{h_{y1}} \\ \alpha_{y2} = \dfrac{l_{y3}}{l_{y2}'} \approx \dfrac{h_{y3}}{h_{y2}} \\ \alpha_{y3} = \dfrac{l_4}{l_{y3}'} \approx \dfrac{h_4}{h_{y3}} \end{cases} \begin{cases} \beta_{x1} = \dfrac{l_{x1}'}{l_{x1}} \\ \beta_{x2} = \dfrac{l_{x2}'}{l_{x2}} \\ \beta_{x3} = \dfrac{l_{x3}'}{l_{x3}} \end{cases} \tag{17}$$

For a reflective optical system, $n_1 = n_2' = n_3 = 1$ and $n_1' = n_2 = n_3' = -1$:

$$\begin{cases} r_{y1} = \dfrac{2\beta_{y1} l_{y1}}{1+\beta_{y1}} \\ r_{y2} = \dfrac{2\alpha_{y1}\beta_{y1}\beta_{y2} l_{y1}}{1+\beta_{y2}} \\ r_{y3} = \dfrac{2\alpha_{y1}\alpha_{y2}\beta_{y1}\beta_{y2}\beta_{y3} l_{y1}}{1+\beta_{y3}} \end{cases} \begin{cases} r_{x1} = \dfrac{2\beta_{x1} l_{x1}}{1+\beta_{x1}} \\ r_{x2} = \dfrac{2\alpha_{x1}\beta_{x1}\beta_{x2} l_{x1}}{1+\beta_{x2}} \\ r_{x3} = \dfrac{2\alpha_{x1}\alpha_{x2}\beta_{x1}\beta_{x2}\beta_{x3} l_{x1}}{1+\beta_{x3}} \end{cases} \begin{cases} d_1 = \beta_1 l_1 - \alpha_1\beta_1 l_1 \\ d_2 = \alpha_1\beta_1\beta_2 l_1 - \alpha_1\alpha_2\beta_1\beta_2 l_1 \\ d_3 = \alpha_1\alpha_2\beta_1\beta_2\beta_3 l_1 - \alpha_1\alpha_2\alpha_3\beta_1\beta_2\beta_3 l_1 \end{cases} \tag{18}$$

Because M_3 is the stop of G1, the chief ray must pass through the vertex of M_3. Here, d_2 can be obtained using ray tracing, and α_{y2} can be calculated as follows:

$$\alpha_{y2} = 1 - \frac{d_2}{\alpha_{y1}\beta_{y1}\beta_{y2} l_{y1}} \tag{19}$$

Additionally, G1, as the anamorphic group, must satisfy some constraints. The magnification of the front group for the XY direction is 2:1. To make the aberration analysis of the subsequent optical system easier, the XY direction rays will intersect at the same point when passing through G1. The ratio of their entrance pupil diameters in the XY direction is 2:1. The stop shape is circular. After consideration of the constraints above, it can be concluded that:

$$\begin{cases} \alpha_{x1} = \dfrac{4d_2 + \beta_{12}\alpha_{12} l_1}{2\beta_{12} l_{y1}} \\ \alpha_{x2} = \dfrac{\beta_{12}\alpha_{12} l_1}{4d_2 + \beta_{12}\alpha_{12} l_1} \end{cases} \begin{cases} \beta_{x1} = \dfrac{-2\beta_{12}\alpha_{12} d_1}{4d_2 - 2\beta_{12} l_1 + \beta_{12}\alpha_{12} l_1} \\ \beta_{x2} = \dfrac{-4d_2 + 2\beta_{12} l_1 - \beta_{12}\alpha_{12} l_1}{4d_1} \\ \beta_{x3} = 4\beta_{y3} \end{cases} \begin{cases} \beta_{12} = \beta_{y1}\beta_{y2} \\ \alpha_{12} = \alpha_{y1}\alpha_{y2} \end{cases} \tag{20}$$

B. Group 2 and Group 3.

The quantities for these groups are defined as follows: d_4, d_5, and d_6 represent the lens thicknesses from M_4 to M_5, from M_5 to M_6, and from M_6 to the image plane, respectively; h_5 and h_6 represent the paraxial marginal ray heights at M_5 and M_6, respectively; r_4, r_5, and r_6, and k_4, k_5, and k_6 represent the radii of curvature and the cones of M_4, M_5, and M_6, respectively; and l_4, l_5, and l_6, and l'_4, l'_5, and

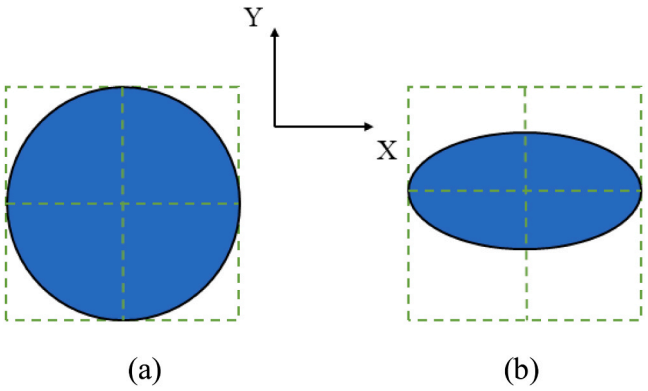

Fig. 5. Entrance pupil shapes for (a) isomorphic system with MAG 4 × and (b) anamorphic system with MAG 4 × /8 × .

$l_6^{'}$ represent the object distances and image distances for M_4, M_5, and M_6, respectively.

Based on the paraxial approximation, we now introduce the following parameters:

$$\alpha_5 = \frac{l_6}{l_5'} \approx \frac{h_6}{h_5} \begin{cases} \beta_4 = \dfrac{l_4'}{l_4} \\ \beta_5 = \dfrac{l_5'}{l_5} \\ \beta_6 = \dfrac{l_6'}{l_6} \end{cases} \tag{21}$$

For a reflective optical system, $n_4' = n_5 = n_6' = 1$ and $n_4 = n_5' = n_6 = -1$, and thus

$$\begin{cases} r_4 = \dfrac{2\alpha_{y1}\alpha_{y2}\alpha_{y3}\beta_{y1}\beta_{y2}\beta_{y3}\beta_4 l_{y1}}{1+\beta_4} \\ r_5 = \dfrac{2\beta_5 l_5}{1+\beta_5} \\ r_6 = \dfrac{2\alpha_5\beta_5\beta_6 l_5}{1+\beta_6} \end{cases} \quad \begin{cases} l_4^{'} = \alpha_1\alpha_2\alpha_3\beta_1\beta_2\beta_3\beta_4 l_1 \\ d_5 = l_4^{'} - d_4 \\ l_5 = d_5 \\ d_6 = \alpha_5\beta_5\beta_6 d_5 \end{cases} \tag{22}$$

To ensure good telecentricity for the system, the radius of curvature of M_6 should be equal to twice the distance between the stop of the latter group and M_6 as far as possible.

C. Entrance pupil shape control and optical pupil matching.

Because the anamorphic optics system has a demagnification of 4 × in the orthogonal scanning direction and 8 × in the scanning direction, the entrance pupil shape of the anamorphic optics system is elliptical when compared with the circular entrance pupil shape of the conventional optics system, as illustrated in Fig. 5. In Section 2.1 part A, paraxial theory is used to consider the ratios of the entrance pupil diameters in both XY directions, but the paraxial theory contains an approximation and the results deviate from the actual system performance. To ensure that the pupil shape of the initial system is correct, an elliptical pupil is used as an input to perform spatial ray tracing and make the final form of the initial system closer to the actual system. Spatial ray tracing is also applied to determine the stop position. The stop position is determined using the intersection of the true ray tracing of the central field chief ray with the z-axis, and group matching is achieved based on true ray tracing of the central field's chief ray.

3. Initial system solution

After parameterization of the system parameters of the tilted and decentered anamorphic optical system, each group is processed and analyzed using the corresponding aberration theory, and to control the constraints of the obscurations effectively, a mathematical model for parametric design of the tilted and decentered anamorphic optical system is established. This physical model is then transformed into a mathematical model. The evaluation function of this model mainly includes the amount of third-order aberrations, the third-order aberration node behavior, and the constraints. The evaluation function can then be written as:

Table 1
Structural Constraints of the Initial System.

Parameter	Specification
Wavelength	13.5 nm
Numerical aperture	0.55
Image-side field of view	26 mm × 0.5 mm
Demagnification	$M_x = 4, M_y = 8$
Chief Ray Angle on Mask(°)	Y: 6 ± 0.2
Chief Ray Angle on Wafer(mrad)	< 0.2
Image working distance	≥ 30 mm
Total track length	< 2000 mm
Obscuration ratio	< 35%

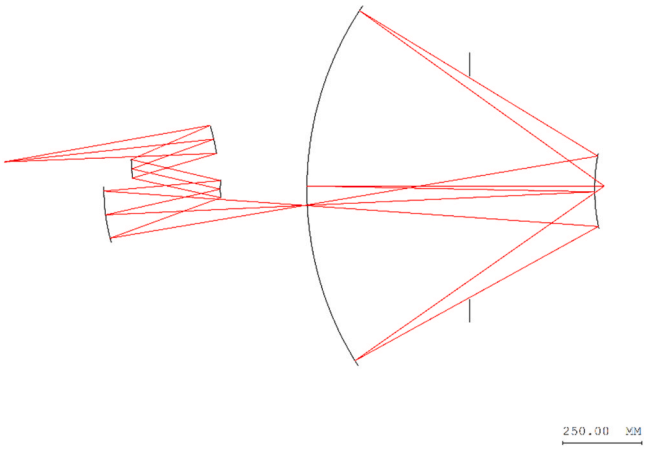

Fig. 6. Initial structure of the tilted and decentered anamorphic optical system.

Table 2
Structural Parameters of the Initial System.

Parameter	Specification
Wavelength	13.5 nm
Numerical aperture	0.55
Image-side field of view	26 mm × 0.5 mm
Demagnification	$M_x = 4, M_y = 8$
Chief Ray Angle on Mask(°)	Y: 6.1
Chief Ray Angle on Wafer (mrad)	0
Image working distance	30 mm
Total track length	1887 mm
Obscuration ratio	24.7%

$$
\begin{aligned}
&F = f(\alpha_{x1..x5}, \alpha_{y1..y5}, \beta_{x1..x6}, \beta_{y1..y6}, k_{x1..x6}, k_{y1..y6}) \\
&= \sum_{i=1}^{16} |\omega_i \cdot D_i| + \left|\omega_{j,1} \cdot \vec{a}_{131}\right| + \left|\omega_{j,2} \cdot \vec{H}_{ast}\right| + \left|\omega_{j,3} \cdot \vec{a}_{220M}\right| + \left|\omega_{j,4} \cdot b_{220M}\right| + \left|\omega_{j,5} \cdot \delta z_{220M}\right| + |\text{constraints}| \\
&= \sum_{i=1}^{16} |\omega_i \cdot D_i| + \left|\omega_{j,1} \cdot \vec{a}_{131}\right| + \left|\omega_{j,2} \cdot \vec{H}_{ast}\right| + \left|\omega_{j,3} \cdot \vec{a}_{220M}\right| + \left|\omega_{j,4} \cdot b_{220M}\right| + \left|\omega_{j,5} \cdot \delta z_{220M}\right| \\
&\quad + \left|\omega_{j,6} \cdot Obscuration\right| + \left|\omega_{j,7} \cdot Obscuration\right| + \left|\omega_{j,8} \cdot BWD\right| + \left|\omega_{j,9} \cdot TEL\right| + \left|\omega_{j,10} \cdot RATIO\right| \\
&+ \left|\omega_{j,11} \cdot APE\right| + \left|\omega_{j,12} \cdot AOI\right| + \left|\omega_{j,13} \cdot DIS\right|
\end{aligned}
\tag{23}
$$

The constraints shown in the equation represent the sums of the constraints listed above. Obscuration, BWD, TEL, RATIO, AOI, APE, and DIS represent the obscuration, the back working distance, the image telecentricity, the obscuration ratio, the maximum aperture, the maximum angle of incidence, and the distances separating the mirrors of the optical system, respectively; in addition, ω denotes the weighting factor. The main constraint indicators for the initial system are listed in Table 1.

The initial system can be obtained by searching for the solution as shown in Fig. 6, and the constraint results for this system are presented in Table 2. The field map of the coma aberration is shown in Fig. 7(a). The nodes of the coma are all close to the field. The

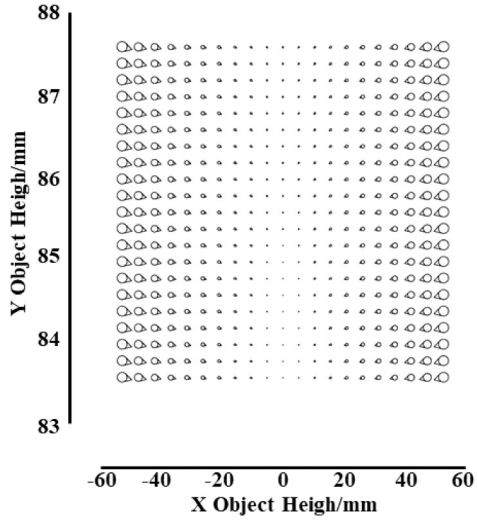

Fig. 7. (a) Coma and (b) astigmatism contributions across the full FOV.

field map of the astigmatism is shown in Fig. 7(b). As a result of the presence of the anamorphic surface in the system, the behavior of the surface's nodes in the field shows node behavior parallel to the Y-axis, as described in Section 2.1. The optical system with the coaxial components has coma and astigmatism nodes in the center of the image plane. These nodes are not close to or within the desired range, which makes it difficult to increase the number of degrees of freedom and reduce the imaging quality when using the tilted and decentered components in the subsequent optimization step.

4. Optimized design

Next, optimization of the initial structure shown above is performed. We fitted the anamorphic aspherical surfaces to symmetric XY polynomial surfaces, which can provide more degrees of freedom for additional aberration corrections. This freeform surface can be expressed as:

$$Z = \frac{cr^2}{1+\sqrt{1-(1+k)c^2r^2}} + \sum_{j=2}^{66} C_j x^m y^n \tag{24}$$

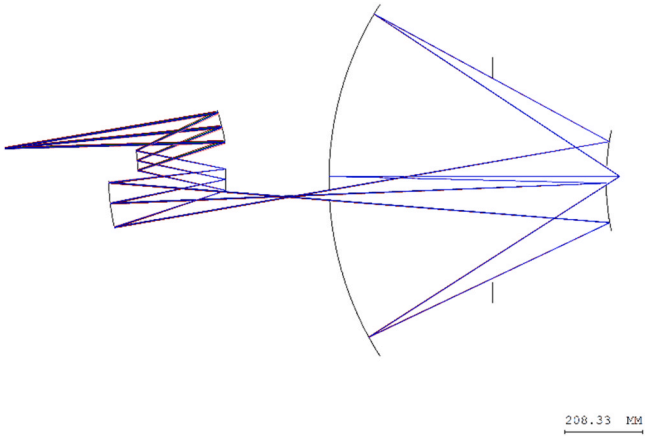

Fig. 8. Optimized results for the tilted and decentered anamorphic optical system.

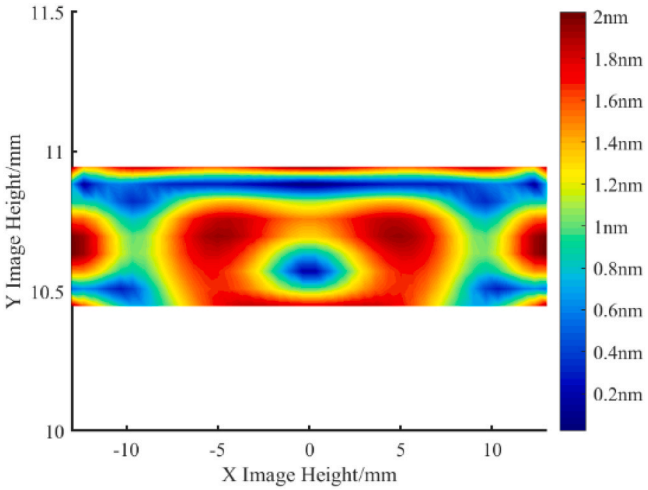

Fig. 9. Distortion over the full image field.

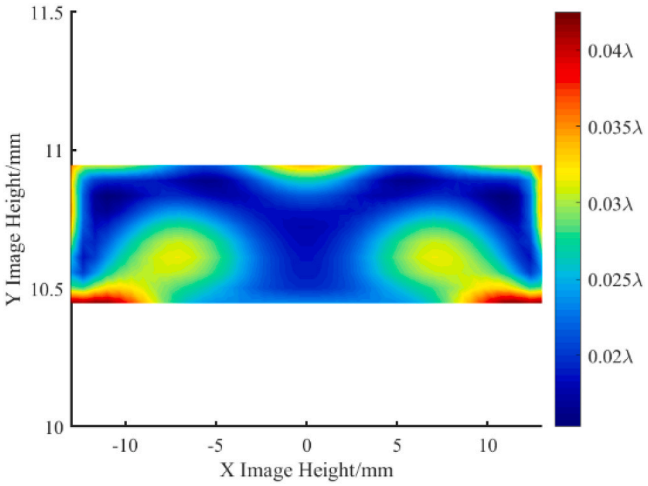

Fig. 10. Wavefront RMS error over the full image field.

Table 3
Optical Characteristics of the Anamorphic Magnification EUV Lithographic Objective.

Parameter	Specification
Wavelength	13.5 nm
Numerical aperture	0.55
Demagnification	$M_x = 4, M_y = 8$
Image-side field of view	26 mm × 0.5 mm
Chief Ray Angle on Mask(°)	Y: 5.4
Total track length	1648 mm
Image working distance	36 mm
Wavefront error (RMS)	1/40λ
Max distortion	≤ 2 nm
Telecentricity	< 0.2mrad
Obscuration ratio	33%

$$j = \frac{(m+n)^2 + m + 3n}{2} + 1$$

Polynomial coefficients with x as an even order, the tilted and decentered elements in the Y-Z plane, and the distances between mirrors are used as optimization variables for the optimization process. The resulting design of the tilted and decentered anamorphic optical system is shown in Fig. 8, and the results for the specific design parameters are presented in Table 1. The image NA is 0.55. The exposure field dimensions at the wafer are 26 mm × 0.5 mm. The total working distance is 1648 mm. The maximum distortion is 2 nm and the integrated wavefront error for the full field is 0.025λ RMS. Fig. 9 shows the distortion distribution over a full image field. Fig. 10 shows the distribution of the wavefront RMS error over a full image field.

5. Summary

To obtain the initial structure with the additional degrees of freedom required to enable realization of a very small wave aberration system, the high-NA EUV lithography projection objective adds a tilted and decentered element to its anamorphic optical system. For design of this complex optical system, this paper proposes an initial system construction method for the tilted and decentered anamorphic optical system that focuses on the problems of aberration balance and constraint control of the anamorphic optical system and the tilted and decentered system during the process of initial system construction. First, the system elements are grouped based on the magnification requirements. An aberration analysis of the anamorphic optical system is performed using vector aberration theory. The nodal behavior of the tilted and decentered optical system is also analyzed using nodal aberration theory. Spatial ray tracing is used to control the entrance pupil shape of the anamorphic optical system and to complete pupil matching between the groups. Using paraxial theory, the system structure parameters are parametrically repaired. We then characterize the constraint parameters and establish a mathematical model of the initial structure of the tilted and decentered anamorphic optical system. Finally, an initial structure that satisfies the aberration balance and multiple constraint control requirements is obtained by solving the mathematical model, which then provides a design starting point for subsequent optimization. The initial structure of the EUV tilted and decentered anamorphic objective with NA= 0.55 was designed using this method, and the wavefront RMS error was better than 0.025λ.

This method is not only applicable to the design of initial structures for high-NA EUV lithography objectives but also can be used to provide initial structures for tilted and decentered optical systems in other fields that satisfy the aberration balance requirement and multiple constraints.

Disclosures

The authors declare no conflicts of interest.

Funding

National Science and Technology Major Project (2018ZX02102002).

Declaration of Competing Interest

The authors declare that they have no known competing financial interests or personal relationships that could have appeared to influence the work reported in this paper.

Data Availability

The data that has been used is confidential.

References

1 J. Van Schoot, K. van Ingen Schenau, C. Valentin, S. Migura, March). EUV lithography scanner for sub-8nm resolution, Extrem. Ultrav. (EUV) Lithogr. VI Vol. 9422 (2015) 449–460 (SPIE).
2 J.T. Neumann, M. Rösch, P. Gräupner, S. Migura, B. Kneer, W. Kaiser, K. van Ingen Schenau, March). Imaging performance of EUV lithography optics configuration for sub-9nm resolution, Extrem. Ultrav. (EUV) Lithogr. VI Vol. 9422 (2015) 471–479 (SPIE).
3 J. Van Schoot, S. Lok, E. van Setten, R. Maas, K. Troost, R. Peeters, J. Finders, J. Stoeldraijer, J. Benschop, P. Graeupner, P. Graeupner, P. Kuerz, W. Kaiser, January). High-NA EUV lithography exposure tool: advantages and program progress, in: In Extreme Ultraviolet Lithography 2020, Vol. 11517, 2021, pp. 76–89 (SPIE).
4 H.J. Mann, W. Ulrich, October). Reflective high-NA projection lenses, Opt. Des. Eng. II Vol. 5962 (2005) 332–339 (SPIE).
5 Y. Liu, Y. Li, Z. Cao, Design of anamorphic magnification high-numerical aperture objective for extreme ultraviolet lithography by curvatures combination method, Appl. Opt. 55 (2016) 4917–4923.
6 Y. Wu, L. Wang, X. Zhang, J. Yu, B. Yu, C. Jin, Design method for an off-axis reflective anamorphic optical system with aberration balance and constraint control, Appl. Opt. 60 (2021) 4557–4566.
7 S. Yuan. Aberrations of anamorphic optical systems [M]. The University of Arizona, 2008.
8 S. Yuan, J. Sasian, Aberrations of anamorphic optical systems. II. Primary aberration theory for cylindrical anamorphic systems, Appl. Opt. 48 (2009) 2836–2841.
9 S. Yuan, J. Sasian, Aberrations of anamorphic optical systems. I: the first-order foundation and method for deriving the anamorphic primary aberration coefficients, Appl. Opt. 48 (2009) 2574–2584.
10 S. Yuan, J. Sasian, Aberrations of anamorphic optical systems III: the primary aberration theory for toroidal anamorphic systems, Appl. Opt. 49 (2010) 6802–6807.
11 D. Ochse, June). Aberration fields of anamorphic systems, in: In Optical Design and Engineering VII, Vol. 10690, 2018, pp. 284–292 (SPIE).
12 Kevin P. Thompson, Tobias Schmid, Ozan Cakmakci, Jannick P. Rolland, Real-ray-based method for locating individual surface aberration field centers in imaging optical systems without rotational symmetry, J. Opt. Soc. Am. A 26 (2009) 1503–1517.
13 Kevin Thompson, Description of the third-order optical aberrations of near-circular pupil optical systems without symmetry, J. Opt. Soc. Am. A 22 (2005) 1389–1401.